THE JOURNAL OF PHYSICAL CHEMISTRY B

Article

pubs.acs.org/JPCB

Gas-Phase Conformations and Energetics of Protonated 2′-Deoxyadenosine and Adenosine: IRMPD Action Spectroscopy and Theoretical Studies

R. R. Wu,[†] Bo Yang,[†] G. Berden,[‡] J. Oomens,[‡,§] and M. T. Rodgers*[,†]

[†]Department of Chemistry, Wayne State University, Detroit, Michigan 48202, United States

[‡]Radboud University Nijmegen, Institute for Molecules and Materials, FELIX Facility, Toernooiveld 7, 6525 ED Nijmegen, The Netherlands

[§]van't Hoff Institute for Molecular Sciences, University of Amsterdam, Amsterdam, The Netherlands

Supporting Information

ABSTRACT: The gas-phase conformations of protonated 2′-deoxyadenosine, $[dAdo+H]^+$, and its RNA analogue protonated adenosine, $[Ado+H]^+$, generated upon electrospray ionization are examined using infrared multiple photon dissociation (IRMPD) action spectroscopy techniques and supported by complementary theoretical electronic structure calculations. IRMPD action spectra are measured over the IR fingerprint region using the FELIX free-electron laser and the hydrogen-stretching region using an optical parametric oscillator/amplifier laser system. The measured IRMPD spectra are compared to linear IR spectra predicted for the stable low-energy conformations of $[dAdo+H]^+$ and $[Ado+H]^+$ computed at the B3LYP/6-311+G(d,p) level of theory to determine the preferred site of protonation and to identify the structures populated in the experiments. N3 is found to be the most favorable site of protonation for both $[dAdo+H]^+$ and $[Ado+H]^+$, whereas conformers protonated at the N1 and N7 positions are much less stable by >25 kJ/mol. The 2′-hydroxyl substituent of Ado does not lead to a significant change in the structure of the ground-state conformer of $[Ado+H]^+$ as compared to that of $[dAdo+H]^+$, except that it provides additional stabilization via the formation of an O2′H···O3′ hydrogen bond. Therefore, $[dAdo+H]^+$ and $[Ado+H]^+$ exhibit highly parallel IRMPD spectral features in both the fingerprint and hydrogen-stretching regions. However, the additional 2′-hydroxyl substituent markedly affects the IRMPD yield of the measured IR bands. The spectral signatures in the hydrogen-stretching region provide complementary information to that of the fingerprint region and enable facile differentiation of the conformers that arise from different protonation sites. In spite of the relative gas-phase stabilities of the N3 and N1 protonated conformers, present results suggest that both are accessed in the experiments and contribute to the measured IRMPD spectrum, indicating that the relative stabilities in solution also influence the populations generated by electrospray ionization.

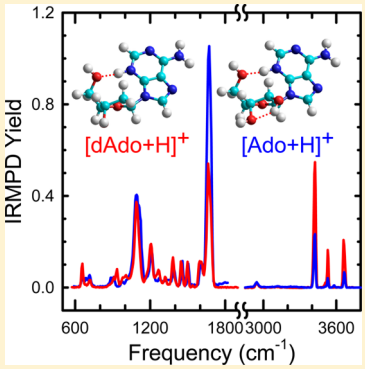

INTRODUCTION

DNA and RNA are essential for the storage and expression of all biological information. The primary sequence as well as the higher-order structure of DNA and RNA determine their biochemical properties and functions. In particular, hydrogen-bonding interactions[1,2] play important roles in determining higher-order structures of DNA and RNA polymers. The pH greatly influences hydrogen-bonding interactions within DNA and RNA. Variations in pH alter structural features and induce changes in the biochemical properties and functions of DNA and RNA. For example, in acidic environments, adenine (A) may be protonated and form noncanonical A^+···C and A^+···G base pairs rather than the canonical A···T base pair.[3] It has been found that in these base pairs adenine is present in a syn orientation rather than the anti orientation as found in standard Watson−Crick base pairs. The 2′-hydroxyl groups within RNA provide additional opportunities to form novel types of hydrogen-bonding interactions. In particular, the 2′-hydroxyl group can participate in sugar-edge base pairing and lead to a multitude of complex tertiary structural motifs.[4] In addition to the vital role that hydrogen-bonding interactions play in maintaining the structures and biochemical properties of DNA and RNA, the puckering of the sugar moiety and the orientation of the base relative to the sugar are also extremely important. This is clearly exemplified by the change from C2′-endo to C3′-endo puckering of the sugar moiety upon transition from the most commonly observed B-form of double-stranded DNA to the A-form of DNA and RNA, which are generally observed in RNA−DNA and RNA−RNA complexes.[5] Similarly, the change from C2′-endo to C3′-endo puckering of the sugar together with the rotation of the guanine residues from "anti" to "syn" conformations in the transition

Received: September 12, 2014
Revised: January 25, 2015
Published: January 26, 2015

DOI: 10.1021/jp509267k
J. Phys. Chem. B 2015, 119, 2795−2805

from the B-form to the less common Z-form of DNA.[6] For these reasons, a greater appreciation of the structural features of the DNA and RNA nucleosides and how they are influenced by the local environment as the basic constituents of nucleic acids is crucial to understanding and elucidating more complex DNA and RNA structures and their functional properties.

The fundamental importance of nucleosides extends beyond their primary role in cellular biology as basic components of nucleic acids. Nucleosides also play roles as cancer biomarkers,[7,8] and many synthetic modified nucleosides have been used as chemotherapeutic and antiviral agents.[9,10] DNA and RNA structures[11−33] have been investigated for more than six decades. However, studies designed to probe the structures of the canonical DNA and RNA nucleosides are rather limited.[34−36] Among the common nucleosides, 2′-deoxyadenosine (dAdo) and its RNA analogue adenosine (Ado), shown in Figure 1, are of great interest because dAdo participates in cellular respiration, protein synthesis, and molecular recognition,[37,38] whereas Ado is the major component of mono-, di-, and triphosphorylated adenosine, AMP, ADP, and ATP, which are the sources of energy required for the activation of many enzymatic transformations.[39] In addition, the nucleobase adenine in both dAdo and Ado exhibits high UV photostability, a characteristic that is essential to the preservation of genetic information.[40] The 3′,5′-cyclic monophosphate of adenosine (cAMP) plays a crucial role in controlling and mediating the actions of various peptidic hormones.[41] Nicotinamide adenine dinucleotide (NAD)[42] and flavin adenine dinucleotide (FAD)[43] are directly implied in redox reactions.

Studies[44−46] of the intrinsic structure of the neutral and protonated forms of dAdo and Ado have been performed.

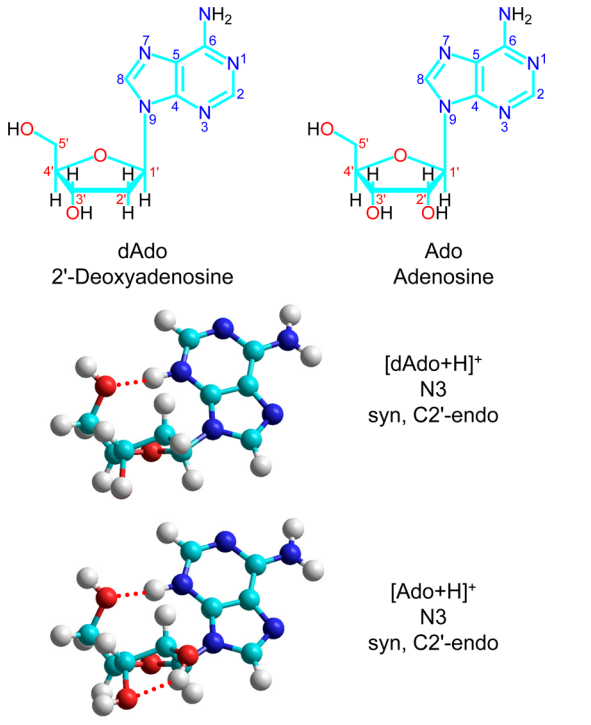

Figure 1. Chemical structures of 2′-deoxyadenosine (dAdo) and adenosine (Ado). Ground-state structures of $[dAdo+H]^+$ and $[Ado+H]^+$ predicted at the B3LYP/6-311+G(2d,2p)//B3LYP/6-311+G(d,p) and MP2(full)/6-311+G(2d,2p)//B3LYP/6-311+G(d,p) levels of theory. The preferred site of protonation, nucleobase orientation, and sugar puckering are indicated in the figure.

Touboul and co-workers[46] studied protonation thermochemistry of adenosine using the extended kinetic method coupled with density functional theory calculations. They reported a gas phase proton affinity (PA) of 979 ± 1 kJ/mol for adenosine and determined N3 as the most favorable site of protonation. In the present work, synergistic infrared multiple photon dissociation (IRMPD) action spectroscopy experiments and electronic structure calculations are employed to probe the effect of protonation on the structures and stabilities of dAdo and Ado. Comparison between the structures as well as the calculated linear IR and measured IRMPD spectra of $[dAdo+H]^+$ and $[Ado+H]^+$ allow the effect of the 2′-hydroxyl moiety on the structure and IR spectral features of the measured IRMPD spectra to be elucidated. The resonant vibrational modes, preferred sites of protonation, and the low-energy conformers that are populated in the experiments are thus determined via comparison between the calculated IR and measured IRMPD spectra.

EXPERIMENTAL AND COMPUTATIONAL SECTION

Mass Spectrometry and Photodissociation. IRMPD action spectra of the protonated forms of 2′-deoxyadenosine and adenosine, $[dAdo+H]^+$ and $[Ado+H]^+$, were measured using a 4.7 T Fourier transform ion cyclotron resonance mass spectrometer (FT-ICR MS) that has been described in detail.[47−49] Photodissociation is achieved over the IR fingerprint region using the widely tunable free-electron laser for infrared experiments (FELIX)[50] and over the hydrogen-stretching region using an OPO/OPA laser system. The nucleosides were purchased from Sigma-Aldrich. Approximately 0.5 mM of the nucleoside, dAdo or Ado, along with 3 mM of acetic acid were dissolved in a 50%:50% MeOH-H_2O mixture. The solutions were delivered to a Micromass "Z-spray" electrospray ionization (ESI) source using a syringe pump operated at a flow rate in the range between 2.7 and 5.8 μL/min. The ions emerging from the spray were accumulated in an rf hexapole ion trap for approximately 3−8 s prior to pulsed extraction through a quadrupole deflector. Trapping conditions were optimized to maximize the single intensity and minimize fragmentation of the protonated nucleoside, $[dAdo+H]^+$ or $[Ado+H]^+$. The observed degree of fragmentation was very low, suggesting that the ions were rapidly cooled to room temperature by collisions in the hexapole. The next bunch of ions was accumulated in the hexapole trap while the extracted ions were injected into the ICR cell of the FT-ICR MS. The ions were captured in the ICR cell by electrostatic switching of the dc bias of the octopole.[48] The ions were stored for at least 300 ms in the ICR cell at ~10^{-8} Torr to cool to room temperature by radiative emission. The protonated nucleoside, either $[dAdo+H]^+$ or $[Ado+H]^+$, was isolated using stored waveform inverse Fourier transform (SWIFT) techniques and irradiated continuously by the free-electron laser for 2.5 to 3 s to induce IR photodissociation over the wavelength range between ~18.0 and ~5.2 μm, corresponding to the range of vibrational frequencies extending from ~550 to ~1920 cm^{-1}. In separate experiments, the ions were irradiated using a benchtop optical parametric oscillator/amplifier (OPO/OPA) system that generates radiation in the hydrogen stretching region for 4−8 s over the wavelength range extending from ~3.6 to ~2.6 μm, corresponding to vibrational frequencies in the range between ~2800 and ~3850 cm^{-1} to provide complementary spectral information.

DOI: 10.1021/jp509267k
J. Phys. Chem. B 2015, 119, 2795−2805

Computational Details. The chemical structures of neutral dAdo and Ado are displayed in Figure 1. In both structures shown in this figure, the nucleobase, adenine, is shown in the anti orientation relative to the glycosidic bond. The most favorable protonation sites, N1, N3, and N7, of $[dAdo+H]^+$ and $[Ado+H]^+$ were carefully examined. Candidate structures for the N1, N3, and N7 protonated forms of both $[dAdo+H]^+$ and $[Ado+H]^+$ were generated by simulated annealing using HyperChem[51] with the Amber force field. Each structure was subjected to 300 cycles of simulated annealing. Each cycle involved 0.3 ps of thermal heating from 0 to 1000 K. The protonated nucleoside was then allowed to sample conformational space at 1000 K for 0.2 ps. The protonated nucleoside was then gradually cooled to 0 K over a period of 0.3 ps. The Amber force field was then used to optimize the resulting structure. A molecular mechanics calculation was performed every 0.001 ps in each cycle, and a snapshot of the resulting structure was saved and used to initiate the next cycle. The structures chosen for higher level optimization and energetic characterization were based primarily on their relative stabilities determined in the simulated annealing process. However, additional higher energy structures were also included to comprehensively investigate all of the various combinations of the sites of protonation (N1, N3, and N7), puckering of the sugar moiety (C2′-endo and C3′-endo) and nucleobase orientation (anti and syn). Geometry optimizations, frequency analyses, and single-point energy calculations of all candidate structures were performed using Gaussian 09.[52] These structures were first optimized at the B3LYP/6-31G(d) level of theory to facilitate convergence to a stable minimum. The resulting structures were reoptimized using the 6-311+G(d,p) basis set to improve the description of the hydrogen-bonding interactions that stabilize these systems. Frequency analyses of these latter structures, again using the 6-311+G(d,p) basis set, were performed to determine vibrational frequencies and IR intensities of the optimized structures for use in calculating the theoretical linear IR spectra. Single point energies were calculated at the B3LYP/6-311+G(2d,2p) and MP2(full)/6-311+G(2d,2p) levels of theory to determine the relative stabilities of the stable low-energy conformers found using these procedures. To examine the effects of solvation on the relative stabilities of the most stable N3 and N1 protonated conformers, limited calculations at the same levels of theory using a polarizable continuum model (PCM) in water were also performed. Zero-point energy (ZPE) corrections as well as thermal conversions to 298 K were included using vibrational frequencies calculated at the B3LYP/6-311+G(d,p) level of theory. The vibration frequencies in the fingerprint region were scaled by a factor of 0.98 and by a factor of 0.957 for the hydrogen stretching region. The calculated vibrational frequencies are convoluted with a 20 cm^{-1} fwhm Gaussian line shape over the fingerprint region, whereas a 10 cm^{-1} fwhm Gaussian line shape is used for the hydrogen-stretching region to model the observed experimental broadening in these spectral regions.

RESULTS

IRMPD Action Spectroscopy. In both the fingerprint and hydrogen-stretching regions, the only photodissociation pathway observed for both $[dAdo+H]^+$ and $[Ado+H]^+$ involves *N*-glycosidic bond cleavage, resulting in production of protonated adenine, $[Ade+H]^+$, with concomitant elimination of the neutral sugar moiety. The IRMPD yield was calculated as the ratio of the intensity of the $[Ade+H]^+$ product and the total ion intensity after laser irradiation at each wavelength as expressed below in eq 1.

$$\text{IRMPD yield} = I_{[Ade+H]^+}/(I_{[Ade+H]^+} + I_{[Nuo+H]^+}) \quad (1)$$

To correct for variations in the laser power as a function of photon energy, the IRMPD yield was adjusted via linear normalization with the FEL or OPO laser power. IRMPD action spectra were obtained for each protonated nucleoside, $[dAdo+H]^+$ and $[Ado+H]^+$, over the range of vibrational frequencies extending from ~550 to 1920 cm^{-1} and from ~2800 to 3800 cm^{-1} and are compared in Figure 2. The measured IRMPD spectra of $[dAdo+H]^+$ and $[Ado+H]^+$ exhibit highly parallel spectral features in both the fingerprint and hydrogen-stretching regions. The affect of the 2′-hydroxyl substituent is primarily seen in the relative intensities of the observed spectral features. In the fingerprint region above ~1500 cm^{-1}, $[Ado+H]^+$ produces higher IRMPD yield than $[dAdo+H]^+$, whereas in the hydrogen-stretching region above ~3400 cm^{-1}, $[dAdo+H]^+$ produces greater IRMPD yield than $[Ado+H]^+$.

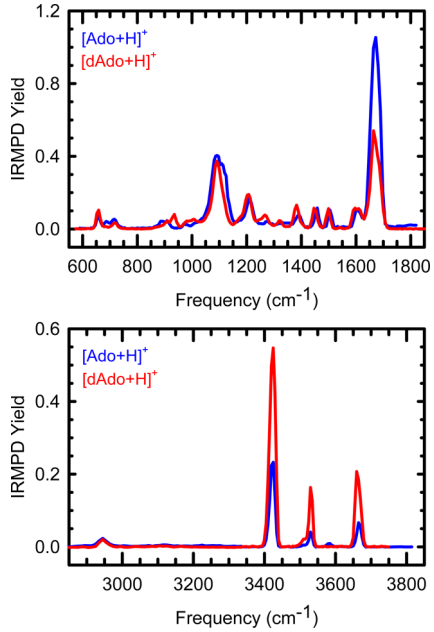

Figure 2. IRMPD action spectra of $[dAdo+H]^+$ and $[Ado+H]^+$ in the fingerprint and hydrogen-stretching regions.

Theoretical Results. The ground-state conformers of $[dAdo+H]^+$ and $[Ado+H]^+$ calculated at the B3LYP/6-311+G(2d,2p)//B3LYP/6-311+G(d,p) and MP2(full)/6-311+G(2d,2p)//B3LYP/6-311+G(d,p) levels of theory are shown in Figure 1. The same ground structures are predicted by B3LYP and MP2 theories for $[dAdo+H]^+$ and $[Ado+H]^+$, which in turn are highly parallel to one another. N3 is the preferred site of protonation for both $[dAdo+H]^+$ and $[Ado+H]^+$. In the ground conformers, adenine takes on a syn orientation about the glycosidic bond, and the sugar puckering is C2′-endo. The 2′-hydroxyl of $[Ado+H]^+$ does not exert a significant effect on the overall structure except that the orientation of the 3′-hydroxyl substituent changes to enable formation of a hydrogen-bonding interaction between the 2′- and 3′-hydroxyl substituents. The 2′-hydroxyl substituent

DOI: 10.1021/jp509267k
J. Phys. Chem. B 2015, 119, 2795−2805

Table 1. Relative Enthalpies and Free Energies of Stable Low-Energy Conformers of $[dAdo+H]^+$ and $[Ado+H]^+$ at 0 and 298 K in kJ/mol[a]

species	conformer	B3LYP			MP2(full)		
		ΔH_0	ΔH_{298}	ΔG_{298}	ΔH_0	ΔH_{298}	ΔG_{298}
$[dAdo+H]^+$	N3A	**0.0**	**0.0**	**0.0**	**0.0**	**0.0**	**0.0**
	N3B	4.8	5.3	3.6	8.2	8.7	7.0
	N3C	12.1	12.2	12.1	12.8	12.9	12.8
	N1A	28.5	29.9	25.3	32.5	33.9	29.3
	N1B	31.6	33.4	27.9	37.2	39.0	33.4
	N3D	32.0	33.1	28.3	39.1	40.2	35.3
	N3E	36.0	37.0	31.3	43.4	44.4	38.6
	N7A	37.6	39.7	33.6	45.5	47.6	41.5
	N1C	42.5	43.0	40.9	41.9	42.4	40.3
	N7B	60.9	62.1	58.8	63.5	64.7	61.4
$[Ado+H]^+$	N3A	**0.0**	**0.0**	**0.0**	**0.0**	**0.0**	**0.0**
	N3B	1.9	1.9	2.4	0.6	0.6	1.1
	N3C	3.4	3.6	2.7	5.0	5.1	4.2
	N3D	6.6	6.8	4.7	8.9	9.1	7.0
	N3E	7.2	7.9	5.3	10.3	10.9	8.4
	N3F	14.1	14.7	10.1	22.1	22.7	18.2
	N3G	13.2	13.6	12.3	14.9	15.4	14.1
	N1A	25.1	26.5	21.8	28.6	30.0	25.4
	N1B	30.2	31.6	26.9	33.9	35.3	30.6
	N1C	36.6	36.8	35.2	35.7	36.0	34.4
	N1D	39.0	40.0	35.9	38.2	39.2	35.2
	N7A	40.5	42.3	37.2	46.2	48.1	42.9
	N7B	42.3	43.6	38.9	44.6	45.9	41.2
	N7C	52.3	53.0	50.8	54.8	55.5	53.3

[a]Energetics based on single-point energy calculations performed at the B3LYP/6-311+G(2d,2p) and MP2(full)/6-311+G(2d,2p) levels of theory, including ZPE and thermal corrections based on the B3LYP/6-311+G(d,p) optimized structures and vibrational frequencies.

appears to strengthen the C1′−N9 glycosidic bond as it contracts from 1.465 Å in $[dAdo+H]^+$ to 1.459 Å in $[Ado+H]^+$. Although this contraction of the glycosidic bond is relatively small, it is consistent across analogous low-energy conformers found for $[dAdo+H]^+$ versus $[Ado+H]^+$. The orientation of adenine about the glycosidic bond changes by only 0.2° as evidenced by the ∠C4N9C1′C2′ dihedral angle, which decreases from −72.0° for $[dAdo+H]^+$ to −71.8° for $[Ado+H]^+$. The O2′H···O3′ hydrogen-bonding interaction leads to a small change in the orientation of the nucleobase and results in a slight increase in the $N3H^+$···O5′ hydrogen bond length from 1.801 Å in $[dAdo+H]^+$ to 1.830 Å in $[Ado+H]^+$. This hydrogen-bonding interaction does not significantly affect the C2′-endo puckering of the sugar moiety as the ∠C1′C2′C3′C4′ dihedral angle changes by less than 1° and is −30.2° in $[dAdo+H]^+$ versus −30.9° in $[Ado+H]^+$. This hydrogen-bonding interaction also has almost no effect on the orientation of the 5′-hydroxymethyl substituent as the ∠O5′C5′C4′O4′ dihedral angles of $[dAdo+H]^+$ and $[Ado+H]^+$ changed by only 0.1° and are −60.4° and −60.3°, respectively.

The relative 0 and 298 K enthalpies and 298 K Gibbs free energies of the stable low-energy conformers of $[dAdo+H]^+$ and $[Ado+H]^+$ are given in Table 1 for all three favorable protonation sites. Structures of the low-energy conformers of $[dAdo+H]^+$ and $[Ado+H]^+$ protonated at N3, N1, and N7 and their relative free energies at 298 K are shown in Figures S1 and S2 of the Supporting Information. The relative stabilities of these low-energy conformers are highly dependent on the site of protonation. The conformers protonated at N1 are >20 kJ/mol higher in free energy than the N3 protonated ground conformers, whereas those protonated at N7 are >30 kJ/mol less stable than the N3 protonated ground conformers. The low-energy conformers displayed in Figures S1 and S2 of the Supporting Information have been chosen primarily based on their computed relative stabilities, but also include all possible combinations of the favorable sites of protonation, nucleobase orientations, and sugar configurations. Conformers protonated at N3 favor the syn orientation of the nucleobase. Therefore, N3 protonated syn conformers exhibiting both C2′-endo and C3′-endo puckering are shown for comparison. The N3 protonated conformers with the nucleobase in an anti configuration prefer C2′-endo puckering of the sugar moiety. The N1 and N7 protonated conformers shown in Figures S1 and S2 of the Supporting Information exhibit both anti and syn orientations of the nucleobase with their preferred sugar puckering. The 2′-hydroxyl substituent provides additional opportunities for hydrogen-bonding interactions with adenine, and multiple favorable orientations of 2′- and 3′-hydroxyl substituents are found. Therefore, a larger number of stable low-energy conformers of $[Ado+H]^+$ are found and compared here. A detailed description of the low-energy conformers displayed in Figures S1 and S2 is given in the Supporting Information.

N3 Protonated Conformers. Both $[dAdo+H]^+$ and $[Ado+H]^+$ show a preference for a syn orientation of adenine, which enables formation of a strong $N3H^+$···O5′ hydrogen-bonding interaction and leads to C2′-endo puckering of the sugar moiety. The relative free energies of **N3A** and **N3B** of $[dAdo+H]^+$ and **N3A**, **N3B**, **N3C**, and **N3E** of $[Ado+H]^+$ suggest that C2′-endo is favored over C3′-endo puckering. When the sugar puckering is C2′-endo, the 2′- and 3′-hydroxyl

DOI: 10.1021/jp509267k
J. Phys. Chem. B 2015, 119, 2795−2805

substituents are preferentially oriented down and away from the adenine residue, whereas conformers that exhibit C3′-endo puckering are more stable when both hydroxyl groups are pointing up and away from the adenine residue. The **N3D** conformer of $[dAdo+H]^+$ has the nucleobase in an anti configuration and is computed to be >25 kJ/mol less favorable than the ground **N3A** conformer where the nucleobase is in a syn configuration, indicating that the rotation of the nucleobase which enables formation of the $N3H^+\cdots O5'$ hydrogen bond provide significant stabilization of the nucleoside. In contrast, the additional 2′-hydroxyl substituent facilitates formation of the $N3H^+\cdots O2'H\cdots O3'$ dual hydrogen-bonding interaction when the nucleobase is in an anti orientation. Therefore, the **N3D** conformer of $[Ado+H]^+$ with the nucleobase in an anti configuration is only 4.7 kJ/mol (B3LYP) and 7.0 kJ/mol (MP2) less stable than the syn-oriented **N3A**.

N1 and N7 Protonated Conformers. Stable conformers of both $[dAdo+H]^+$ and $[Ado+H]^+$ protonated at either N1 and N7 are calculated to be much less stable than N3 protonated conformers. The relative Gibbs free energies of the various N1 and N7 protonated conformers of both $[dAdo+H]^+$ and $[Ado+H]^+$ suggest that N1 protonation is more favorable when the adenine residue is in an anti orientation with C2′-endo sugar puckering, whereas N7 protonation prefers an anti orientation of the adenine residue with C3′-endo puckering of the sugar moeity.

2′- and 3′-Hydroxyl Orientations in $[Ado+H]^+$. Similar to that found for the low-energy conformers of $[Guo+H]^+$,[36] the low-energy conformers of $[Ado+H]^+$ with C2′-endo sugar puckering are more stable when the 2′- and 3′-hydroxyl substituents point down and away from the adenine residue, whereas C3′-endo sugar puckering is more stable when the 2′- and 3′-hydroxyl substituents point up and away from the nucleobase.

Comparison of the Low-Energy Conformers: $[dAdo+H]^+$ versus $[Ado+H]^+$. The stable low-energy conformers of $[dAdo+H]^+$ and $[Ado+H]^+$ shown in Figures S1 and S2 of the Supporting Information exhibit conformational features that are highly parallel. However, the additional $O2'H\cdots O3'$ or $O2'\cdots HO3'$ hydrogen-bonding interactions that the [Ado+H]+ conformers exhibit lead to additional low-energy conformers that are not possible for $[dAdo+H]^+$ (such as the **N3B** and **N3E** conformers), which generally only slightly alter the orientation of the 3′-hydroxyl substituent. Moreover, the 2′-hydroxyl substituent also provides alternative opportunities for hydrogen bonding to the adenine residue, such as found in the **N3D**, **N3F**, **N1D**, and **N7B** conformers of $[Ado+H]^+$.

Comparison of Isolated $[Ade+H]^+$, $[dAdo+H]^+$, $[Ado+H]^+$, and $[dAdo5'p+H]^+$. N3 is found to be the preferred site of protonation for both $[dAdo+H]^+$ and $[Ado+H]^+$, followed by N1 and N7. This trend contrasts that found for protonated adenine, $[Ade+H]^+$, where N1 is found to be the most favorable protonation site.[53,54] The change in the preferred site of protonation is driven by the stabilization provided by the $N3H^+\cdots O5'$ hydrogen-bonding interaction in $[dAdo+H]^+$ and $[Ado+H]^+$, which is clearly not possible for the isolated protonated base. Similar types of intramolecular hydrogen-bonding interactions have been found in the optimized structures of protonated 2-deoxyadenosine-5′-monophosphate, $[dAdo5'p+H]^+$, studied by Bowers and co-workers,[55] where adenine is also protonated at N3, in the syn orientation about the glycosidic bond, but instead hydrogen bonded to the phosphate moiety. Thus, the sugar and phosphate moieties of nucleosides and nucleic acids alter the chemistry of adenine as compared to the isolated nucleobase.

DISCUSSION

Comparison of Measured IRMPD and Calculated IR Spectra of $[dAdo+H]^+$. The measured IRMPD and calculated IR spectra of the most delineative low-energy conformers including each favorable site of protonation, **N3A**, **N1A**, **N3D**, **N3E**, and **N7A** of $[dAdo+H]^+$ in the fingerprint and hydrogen-stretching regions are compared in Figure 3. In the fingerprint region, the strong IR feature predicted at ~1655 cm^{-1} with a shoulder to the red for the N3 protonated conformers, **N3A**, **N3D**, and **N3E**, is shifted to slightly lower frequencies as compared to the measured band at ~1665 cm^{-1}. In contrast, the strong IR feature at ~1680 cm^{-1} with a shoulder to the red predicted for the **N1A** conformer is shifted to a slightly higher frequency than this measured band. Overall, the IR spectra predicted for **N3A**, **N1A**, and **N3D** exhibit good matches with the experimental IRMPD spectrum. The change in the orientation of the adenine residue in the **N3A** versus **N3D** conformers does not significantly affect the calculated band positions in the fingerprint region. The moderately strong band measured at ~1095 cm^{-1}, however, is not well-described by the calculated band of the **N3E** conformer, which is predicted at ~1025 cm^{-1} and may be due to the N3 protonated adenine interacting with the O4′ atom of the sugar rather than the 5′-hydroxyl oxygen atom. This large shift to lower frequencies in the IR feature predicted for **N3E** versus the observed feature suggests that **N3E** is not present in the experiments. The IR band at ~1645 cm^{-1} with a shoulder to the red predicted for the **N7A** conformer is also underestimated by 20 cm^{-1} relative to the observed band at ~1665 cm^{-1}. In addition, the IR absorptions predicted at ~1465 and ~1295 cm^{-1} for **N7A** are not observed in the measured IRMPD spectrum. Therefore, the **N7A** conformer is also not present in the experiments. In the hydrogen-stretching region, the band predicted at ~3052 cm^{-1} for the **N3A** conformer represents the strong harmonic vibration of the shared proton oscillating between N3 and O5′. However, the high degree of anharmonicity associated with this mode leads to very poor theoretical prediction and is therefore not useful for interpretation of the structures populated in the experiments. Similarly, the weak hydrogen-bonding interaction between C8H and O5′ of **N1A** introduces anharmonicity to the C8−H stretch such that the harmonic prediction at ~3093 cm^{-1} for the **N1A** conformer is also not useful for interpretation. The very weak C−H stretches that occur in the hydrogen-stretching region below ~3300 cm^{-1} are also of limited diagnostic utility. Thus, useful comparisons between experiment and theory can only be made above ~3300 cm^{-1}. The calculated bands of **N3A**, **N1A**, and **N3D** match the measured bands above ~3300 cm^{-1} reasonably well. In contrast, there are very large discrepancies between the measured and calculated spectra above ~3300 cm^{-1} for **N3E** and **N7A**, again indicating that these two conformers are not contributing to the measured IRMPD spectrum. Therefore, the **N3A**, **N1A**, and **N3D** conformers are present in the experiments.

The measured IRMPD and calculated IR spectra in the fingerprint and hydrogen-stretching regions for the **N3B**, **N3C**, **N1B**, **N1C**, and **N7B** conformers of $[dAdo+H]^+$ are compared in Figure S3 of the Supporting Information. In the fingerprint region, the IR spectrum predicted for **N3B** is highly parallel to

DOI: 10.1021/jp509267k
J. Phys. Chem. B 2015, 119, 2795−2805

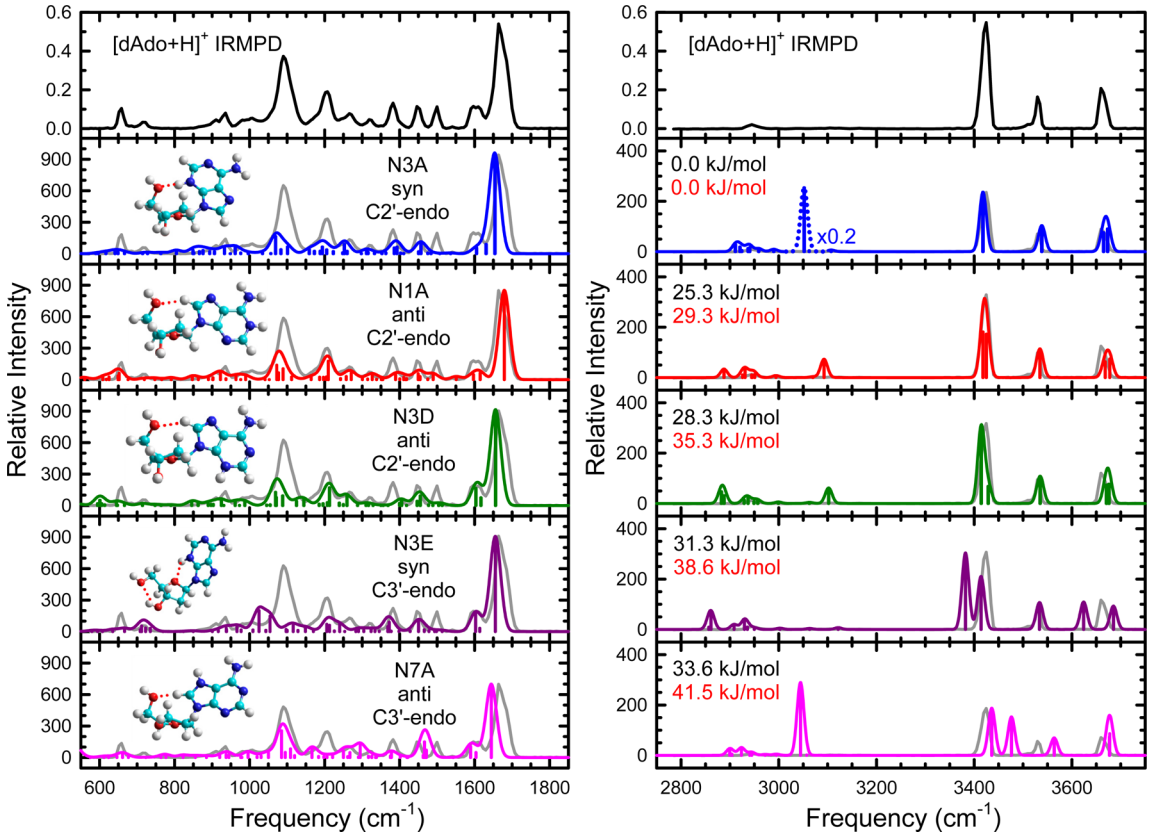

Figure 3. Comparison of the measured IRMPD action spectrum of $[dAdo+H]^+$ with the B3LYP/6-311+G(d,p) optimized structures and predicted linear IR spectra for the ground and representative stable low-energy conformers of $[dAdo+H]^+$. The B3LYP/6-311+G(2d,2p) and MP2(full)/6-311+G(2d,2p) relative Gibbs free energies at 298 K are also shown in black and red, respectively. The site of protonation, nucleobase orientation, and sugar puckering are also indicated for each conformer.

that of **N3A** (Figure 3) and shows reasonably good agreement with the experimental IRMPD spectrum, suggesting that variations in the sugar puckering do not lead to significant differences in the IR spectrum in the fingerprint region. The different orientations of the 5′-hydroxymethyl and 3′-hydroxyl moieties of **N3C** versus those of **N3A** slightly alter the calculated IR features between ~950 and 1100 cm^{-1} (compare Figure 3 and Figures S3 of the Supporting Information). The IR spectrum predicted for **N3C** also exhibits a good match to the experimental IRMPD spectrum in the fingerprint region. The calculated IR spectra of **N1B** and **N1C** exhibit good agreement with the measured IRMPD spectrum and are quite parallel to that of **N1A** (Figure 3), again indicating that the sugar puckering and orientation of the adenine residue are not differentiable from the calculated IR features in the fingerprint region. Similar to **N7A** (Figure 3), the band at ~1650 cm^{-1} with a shoulder to the red predicted for **N7B** occurs at lower frequencies than the measured band at ~1665 cm^{-1}, indicating the absence of **N7B** in the experiments. In the hydrogen-stretching region, the IR spectra predicted for **N3B** and **N3C** exhibit good matches to the experimental IRMPD spectrum. The band predicted at ~3680 cm^{-1} for **N1B** is overestimated versus the measured band at ~3660 cm^{-1}. The band calculated at ~3585 cm^{-1} of **N1C** is not observed in the measured spectrum, and the large discrepancy between the measured and calculated spectra for **N7B** indicate that these two conformers are not populated in the experiments. Therefore, among these five conformers, only **N3B** and **N3C** are populated in the experiments.

In summary, comparison between the measured IRMPD and calculated IR spectra of $[dAdo+H]^+$ in the fingerprint and hydrogen-stretching regions, make it clear that conformers protonated at N7 are not populated in the experiments. Good agreement is achieved for both the N3 and N1 protonated low-energy conformers, **N3A**, **N3B**, **N3C**, **N1A**, and **N3D**, suggesting that all of these conformers may be present in the experiments.

Vibrational Assignments for $[dAdo+H]^+$. On the basis of the IR spectra predicted for the conformers populated in the experiments, the band observed at ~1665 cm^{-1} arises from strong NH_2 scissoring, whereas the shoulder to the red reflects coupled nucleobase stretches. The band observed at ~1205 cm^{-1} is the result of bending of the sugar hydrogen atoms. The moderately strong band observed at ~1095 cm^{-1} is associated with stretching motions of the sugar ring. In the hydrogen-stretching region, the band observed at ~3660 cm^{-1} arises from coupled stretches of the 3′- and 5′-hydroxyl substituents. The moderate IR absorption at ~3530 cm^{-1} represents asymmetric NH_2 stretching, whereas the intense IR absorption at ~3425 cm^{-1} arises from symmetric NH_2 stretching.

Comparison of Measured IRMPD and Calculated IR Spectra of $[Ado+H]^+$. The measured IRMPD and calculated IR spectra of the most delineative low-energy conformers for each favorable site of protonation, **N3A**, **N3D**, **N3F**, **N1A**, and **N7A** of $[Ado+H]^+$ in the fingerprint and hydrogen-stretching regions are compared in Figure 4. **N3A** and **N3D** share the same sugar puckering and 2′- and 3′-hydroxyl orientations but

DOI: 10.1021/jp509267k
J. Phys. Chem. B 2015, 119, 2795−2805

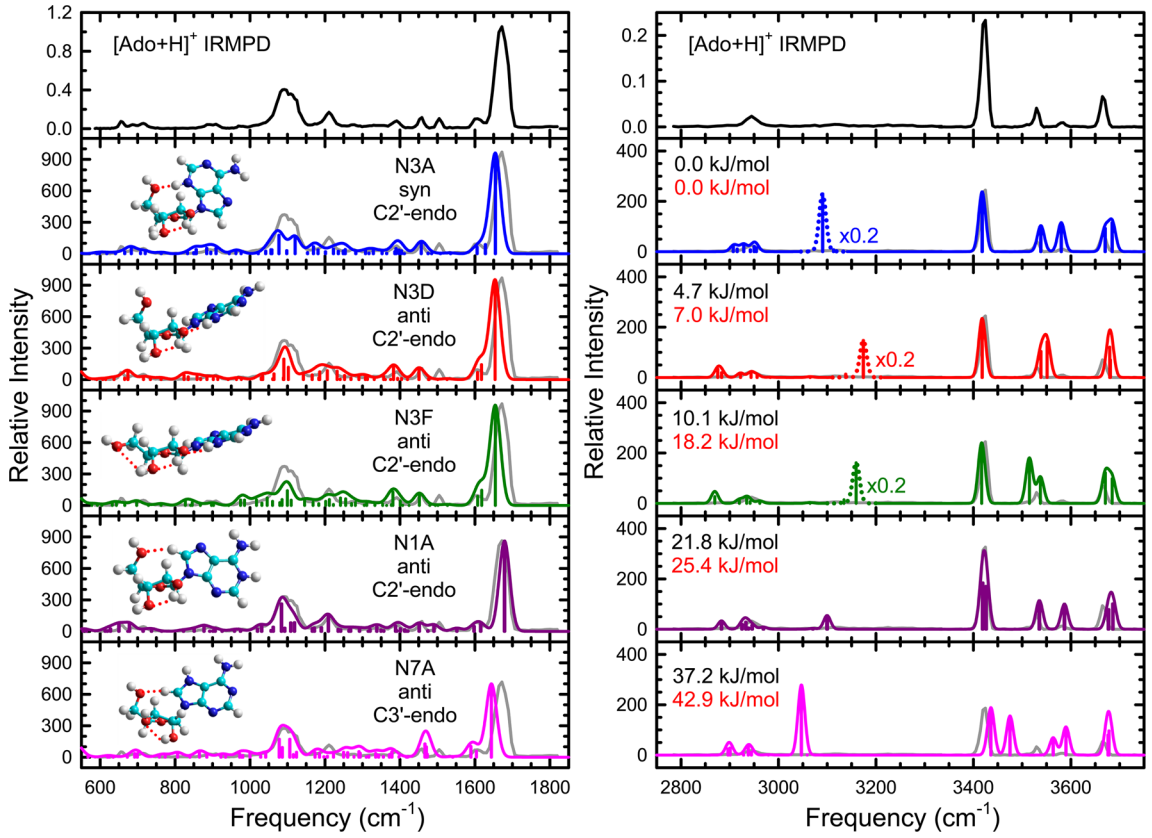

Figure 4. Comparison of the measured IRMPD action spectrum of $[Ado+H]^+$ with the B3LYP/6-311+G(d,p) optimized and predicted linear IR spectra for the ground and representative stable low-energy conformers of $[Ado+H]^+$. The B3LYP/6-311+G(2d,2p) and MP2(full)/6-311+G(2d,2p) relative Gibbs free energies at 298 K are also shown in black and red, respectively. The site of protonation, nucleobase orientation, and sugar puckering are also indicated for each conformer.

exhibit different nucleobase orientations. The $N3H^+\cdots O5'$ hydrogen bond stabilizes the syn-oriented nucleobase of **N3A**, whereas the $N3H^+\cdots O2'H\cdots O3'$ dual hydrogen-bonding interaction stabilizes the anti-oriented nucleobase of **N3D**. However, the different nucleobase orientations are not differentiable in the fingerprint region as their IR features are highly similar. In particular, the IR features above ~1300 cm^{-1} predicted for **N3A** and **N3D** are nearly identical. **N3D** and **N3F** exhibit different orientations of the 5′-hydroxymethyl moiety, which produces discernible IR features below ~1300 cm^{-1}. In particular, small IR features at ~985 cm^{-1} predicted for **N3F** are not predicted for **N3D** and are not observed in the measured IRMPD spectrum. The frequency of the intense IR band at ~1655 cm^{-1} with a shoulder to the red predicted by theory for the **N3A**, **N3D**, and **N3F** conformers is underestimated relative to the measured band at ~1670 cm^{-1}. In contrast, the calculated IR band at ~1680 cm^{-1} of **N1A** occurs at higher frequencies than this measured band, parallel to that found for $[dAdo+H]^+$. Except for the small shifts relative to the band observed at ~1670 cm^{-1}, the IR features predicted for **N3A**, **N3D**, and **N1A** exhibit good agreement with the measured IRMPD features in the fingerprint region. The IR absorption predicted at ~1645 cm^{-1} for **N7A** occurs at much lower frequencies than the measured band at ~1670 cm^{-1}, indicating that **N7A** is not populated in the experiments. The harmonic IR features reflecting the strong N3−H stretch involved in the hydrogen-bonding interactions calculated at ~3090, ~3175, and ~3160 cm^{-1}, respectively, for **N3A**, **N3D**, and **N3F** are not usefully compared for these highly anharmonic modes. Similarly, the calculated harmonic C8−H stretch at ~3100 cm^{-1} and ~3050 cm^{-1}, respectively, for **N1A** and **N7A**, are involved in the $C8H\cdots O5'$ noncanonical hydrogen-bonding interactions, such that these IR features are not well-predicted by the harmonic approximation and thus are not usefully compared to the measured IR features. The IR features observed above ~3300 cm^{-1} in the hydrogen-stretching region are sufficiently diagnostic to elucidate which conformers are populated in the experiments. The IR features observed above ~3300 cm^{-1} are well-reproduced by the calculated IR features of **N3A**. Because of the $N3H^+\cdots O2'H\cdots O3'$ dual hydrogen-bonding interactions present in **N3D** and **N3F**, the weak and moderate IR features measured at ~3580 and ~3530 cm^{-1} are not well-predicted by the calculated IR features of **N3D** and **N3F**. The calculated IR features predicted for **N1A** agree well with the measured IR features in the OPO region. Very large differences between experiment and theory are found for **N7A**, again suggesting the absence of this conformer in the experiments. Therefore, these comparisons imply that the **N3A** and **N1A** conformers are populated in the experiments.

The experimental IRMPD and calculated IR spectra in the fingerprint and hydrogen-stretching regions for the **N3B**, **N3C**, **N3E**, **N3G**, and **N1B** conformers of $[Ado+H]^+$ are compared in Figure S4 of the Supporting Information. Except for small shifts as compared to the band observed at ~1670 cm^{-1}, the IR spectra predicted for **N3B**, **N3C**, **N3E**, and **N1B** exhibit good agreement with the measured IRMPD spectrum in the fingerprint region. The IR feature predicted at ~995 cm^{-1} for

DOI: 10.1021/jp509267k
J. Phys. Chem. B 2015, 119, 2795−2805

N3G does not appear in the observed IRMPD spectrum. The IR spectra predicted for **N3B** and **N3C** in the fingerprint region are quite similar to that of **N3A** (Figure 4), suggesting that changes in the orientations of the 2′- and 3′-hydroxyl substituents and the puckering of the sugar moiety are not easily differentiated by the measured IR features in the fingerprint region. The calculated IR spectrum of **N1B** in the fingerprint region is also parallel to that of **N1A** (Figure 4), again suggesting that the IR features in the fingerprint region are insufficient to distinguish different nucleobase orientations, sugar puckering, and 2′- and 3′-hydroxyl orientations. In the hydrogen-stretching region above ~3300 cm^{-1}, the IR bands predicted at ~3620 cm^{-1} for **N3B** and at ~3610 cm^{-1} for **N3E** are shifted to higher frequencies versus the weak band observed at ~3580 cm^{-1}. The IR features predicted for **N3C** and **N3G** display good agreement with the observed IRMPD features. The band calculated at ~3680 cm^{-1} for **N1B** is also predicted to occur at higher frequencies than the measured band at ~3665 cm^{-1}, whereas all other IR features predicted above ~3300 cm^{-1} for **N1B** exhibit good agreement with the observed IRMPD spectrum. Therefore, among these five low-energy conformers, **N3C** is the only conformer present in the experiments.

The measured IRMPD and calculated IR spectra in the FELIX and OPO regions for the **N1C**, **N1D**, **N7B**, and **N7C** conformers of $[Ado+H]^+$ are compared in Figure S5 of the Supporting Information. In the fingerprint region, the IR spectra predicted for **N1C** and **N1D** exhibit good agreement with the observed IRMPD spectrum. The IR bands at ~1645 cm^{-1} for **N7B** and **N7C** are predicted to appear at much lower frequencies than the measured band at ~1670 cm^{-1}. However, the calculated IR spectra of these four conformers display very poor agreement with the observed IRMPD spectrum in the OPO region. Therefore, none of these four conformers are populated in the experiments.

In summary, comparison between the observed IRMPD and calculated IR spectra of $[Ado+H]^+$ in the fingerprint and hydrogen-stretching regions indicates that conformers protonated at N7 are not present in the experiments. Only **N3A**, **N3C**, and **N1A** are present in the experiments. In both **N3A** and **N3C**, adenine is in the syn orientation interacting with O5′. These results again suggest that C2′-endo puckering is more favorable when the 2′- and 3′-hydroxyl substituents are down and away from the adenine residue, whereas C3′-endo puckering leads to the hydroxyl substituents pointing up and towards the adenine residue. Unlike $[dAdo+H]^+$, no anti-oriented N3 protonated conformers are present in the experiments for $[Ado+H]^+$. Similar to $[dAdo+H]^+$, the **N1A** conformer, having the nucleobase in an anti orientation and exhibiting C2′-endo puckering of the ribose moiety, may be populated in the experiments.

Vibrational Assignments for $[Ado+H]^+$. Comparison of the observed and computed spectra for the conformers populated in the experiments, allows the IRMPD features observed to be assigned. In the fingerprint region, the strong IR band observed at ~1670 cm^{-1} represents strong NH_2 scissoring, whereas the shoulder to the red primarily represents nucleobase stretching. The weak band observed at ~1210 cm^{-1} arises from bending of the hydrogen atoms of the sugar moiety. The broad IR band observed at ~1100 cm^{-1} arises from sugar ring stretches. In the hydrogen-stretching region, the band observed at ~3665 cm^{-1} represents stretching of the 3′- and 5′-hydroxyl substituents. The weak IR feature observed at ~3580 cm^{-1} is assigned to the 2′-hydroxyl stretch. The moderate IR absorption observed at ~3530 cm^{-1} arises from asymmetric NH_2 stretching, whereas the sharp IR absorption observed at ~3425 cm^{-1} results from symmetric NH_2 stretching.

N3 Protonation vs N1 Protonation. It has previously been determined that N1 is the preferred site of protonation adenine[53] and that the most stable conformer of protonated adenine, $[Ade+H]^+$, is the canonical tautomer of adenine protonated at N1.[54] In contrast, present results suggest that in $[dAdo+H]^+$ and $[Ado+H]^+$, N3 protonation enables formation of a $N3H^+\cdots O5'$ hydrogen-bonding interaction via rotation of the adenine residue to the syn orientation, which stabilizes the N3 protonated nucleosides by >20 kJ/mol (B3LYP and MP2) over the most stable N1 protonated conformers. However, comparisons of the observed IRMPD and calculated IR spectra do not enable the presence of the N1 protonated **N1A** conformers of $[dAdo+H]^+$ and $[Ado+H]^+$ to be ruled out. In fact, the IR spectra of the **N1A** conformers exhibit quite good agreement with the observed IRMPD spectrum in the fingerprint region above ~1450 cm^{-1}. This result is somewhat surprising given the relative gas-phase stabilities of these conformers and may be due to differences in the relative stabilities of these conformers in solution as the ions are generated by ESI. To examine this possibility, we computed the relative Gibbs free energies of the **N1A** and **N3A** conformers of $[dAdo+H]^+$ and $[Ado+H]^+$ at the same levels of theory but using a polarizable continuum model in water. Indeed, the **N1A** conformers are found to be significantly more stable in solution than in the gas phase. The **N1A** conformer of $[dAdo+H]^+$ lies 4.5 kJ/mol (B3LYP) and 10.5 kJ/mol (MP2) above **N3A**, whereas the **N1A** conformer of $[Ado+H]^+$ lies only 2.4 kJ/mol (B3LYP) and 7.2 kJ/mol (MP2) above **N3A**. The anti-orientation of the nucleobase in the **N1A** conformers exposes the excess proton to the solvent, facilitating hydrogen-bonding interactions with the solvent that enhance the stability of these conformers relative to the **N3A** conformers. Clearly, the $N3H^+\cdots O5$ hydrogen-bonding interaction plays an important role in stabilizing the **N3A** conformers in the gas phase. As these calculations were performed using the PCM model rather than explicit solvent, the actual stabilization in solution may be even more significant such that the most stable N1 protonated conformers may comprise a larger portion of the population generated upon ESI than suggested by their relative stabilities in the gas phase or in a PCM environment. Similar results were found in a previous IRMPD study of deprotonated *p*-hydroxybenzoic acid where the relative populations of the species generated by deprotonation of the benzoic acid moiety (favored in protic environments) versus phenolic moiety (favored in the gas phase and aprotic environments) was strongly influenced by the solvent(s) used for ESI.[56]

Comparison to IR Studies of Neutral, Protonated, and Metal Cationized Ade. Kleinermanns and co-workers[57] measured the IR spectrum of neutral Ade using IR-UV double-resonance spectroscopy in the range from 3200 to 3700 cm^{-1} and observed only the canonical tautomer of neutral Ade in the experiments. The bands observed at 3452, 3508, and 3569 cm^{-1} were identified as symmetric NH_2, N9−H, and asymmetric NH_2 stretching, respectively. In this work, symmetric and asymmetric NH_2 stretching of $[dAdo+H]^+$ and $[Ado+H]^+$ are observed at ~3425 cm^{-1} and ~3530 cm^{-1}, respectively, corresponding to a shift of ~25 cm^{-1} as compared to that observed for neutral Ade. Rijs and co-

DOI: 10.1021/jp509267k
J. Phys. Chem. B 2015, 119, 2795−2805

workers[58] examined the IR spectrum for neutral Ade in the range extending from 500 to 1750 cm^{-1} using IR-UV ion-dip spectroscopy and the IRMPD spectrum for $[Ade+H]^+$ from 1000 to 1750 cm^{-1} using IRMPD spectroscopy. They again found that the canonical tautomer of neutral Ade as the dominant tautomeric conformation populated in the experiments. However, they were not able to exclude the presence of the noncanonical N7−H tautomer of Ade in their experiments. For $[Ade+H]^+$, their theoretical calculations suggested that the most stable conformer is the noncanonical N7−H neutral tautomer of Ade protonated at N3, which is only 1.0 kJ/mol more stable than the first excited conformer, the canonical N9−H neutral tautomer of Ade protonated at N1. The IR spectrum predicted for the first excited conformer was found to reproduce the measured IR features above ∼1500 cm^{-1} better than the ground conformer and suggested that the solvent preferentially stabilizes the canonical N9−H tautomer of neutral Ade protonated at N1, such that it is the dominant structure generated being by ESI. However, the presence of the noncanonical N7−H tautomer of Ade protonated at N3 could not be not excluded. This result parallels that found here for the protonated nucleosides, $[dAdo+H]^+$ and $[Ado+H]^+$, again suggesting that structures present in solution are maintained in the ESI process in spite of the relative stabilities of these species in the gas phase. Fridgen and co-workers[59] measured the IRMPD spectra of $[Ade+K]^+$ and $[Ade+Cs]^+$ from 3300 to 3600 cm^{-1}. Both theory and experiment find that the preferred structures and site of binding involve bidentate interaction with both N3 and N9 to the noncanonical N7−H tautomer of Ade. The bands observed at 3427 and 3536 cm^{-1} were identified as symmetric and asymmetric NH_2 stretching, respectively, which are consistent with the bands observed for $[dAdo+H]^+$ and $[Ado+H]^+$ in the present work. Thus, these results suggest that alkali metal cationization exerts a similar influence on the symmetric and asymmetric NH_2 stretching modes, which do not appear to be sensitive to the tautomeric conformation of adenine. The band observed at 3488 cm^{-1} in the IRMPD spectra of $[Ade+K]^+$ and $[Ade+Cs]^+$ represents N7−H stretching, which is not observed for $[dAdo+H]^+$ and $[Ado+H]^+$ in the present work and provides additional evidence for the absence of the N7 protonated conformers in our experiments.

CONCLUSIONS

The IRMPD action spectra of the protonated forms of the canonical DNA and RNA nucleosides, 2′-deoxyadenosine and adenosine and $[dAdo+H]^+$ and $[Ado+H]^+$, in the fingerprint region between 550 and1920 cm^{-1} and in the hydrogen-stretching region between 2800 and 3800 cm^{-1} have been measured and compared with linear IR spectra of the stable low-energy conformations predicted for these species calculated at the B3LYP/6-311+G(d,p) level of theory to determine which structures are populated in the experiments. Comparisons between the observed and calculated spectra in the FELIX and OPO regions complement and enhance one another, enabling elucidation of the conformations present in the experiments. In particular, the site of protonation is readily determined from the predicted IR spectra in both regions. N3 protonation allows the formation of a strong intramolecular $N3H^+\cdots O5'$ hydrogen-bonding interaction and is found to be the most stable protonation site for both $[dAdo+H]^+$ and $[Ado+H]^+$, whereas protonation at N1 and N7 is found to be much less favorable. The apparent discrepancies between the observed IRMPD and calculated IR spectra of the N7 protonated conformers in the fingerprint and hydrogen-stretching regions eliminate their presence in the experiments. However, the IR spectra predicted for the N3 and N1 protonated low-energy conformers of $[dAdo+H]^+$ and $[Ado+H]^+$ in the fingerprint region are highly parallel such that they are difficult to distinguish. Comparison between experiment and theory for these systems in the OPO region provides valuable additional information and suggests that conformers protonated at both N3 and N1 are populated in the experiments. On the basis of these comparisons, the **N3A**, **N3B**, **N3C**, **N1A**, and **N3D** conformers of $[dAdo+H]^+$ and the **N3A**, **N3C**, and **N1A** conformers of $[Ado+H]^+$ may be present in the experiments. Both syn nucleobase oriented **N3A**, **N3B**, and **N3C** and anti-nucleobase oriented **N3D** conformers of $[dAdo+H]^+$ may be present in the experiments, whereas only syn nucleobase oriented **N3A** and **N3C** conformers of $[Ado+H]^+$ may be present in the experiments. Both the C2′-endo and C3′-endo puckered N3 protonated conformers, **N3A**, **N3B**, **N3C**, and **N3D** of $[dAdo+H]^+$ and **N3A** and **N3C** of $[Ado+H]^+$ may be present in the experiments, whereas only the anti nucleobase oriented and C2′-endo puckered N1 protonated conformers, **N1A** of $[dAdo+H]^+$ and $[Ado+H]^+$, may be present in the experiments. In spite of the relative stabilities of the N3 and N1 protonated conformers in the gas-phase, the calculated IR spectra of the N1 protonated conformers also exhibit good agreement with the measured IRMPD spectra, particularly above ∼1450 cm^{-1} in the FELIX region and suggest that the structures present in solution are preserved in the ESI process. The puckering of the ribose moiety, C2′-endo versus C3′-endo, is found to exert a strong influence on the preferred orientations of the 2′- and 3′-hydroxyl substituents of $[Ado+H]^+$. In particular, C2′-endo puckering is most stable when the 2′- and 3′-hydroxyl substituents point down and away from the adenine residue (**N3A**), whereas C3′-endo sugar puckering is most stable when the 2′- and 3′-hydroxyl substituents are oriented up and away from the nucleobase (**N3C**). The hydrogen-bond stabilization provided by interactions of the 2′- and 3′-hydroxyl substituents of $[Ado+H]^+$ stiffens the sugar and leaves the nucleobase more flexible such that IVR is more efficient than that of $[dAdo+H]^+$. Therefore, the IRMPD yield of $[Ado+H]^+$ above ∼1500 cm^{-1}, the IR signature region for the adenine residue, exceeds that of $[dAdo+H]^+$. Conversely, the free 3′-hydroxyl of $[dAdo+H]^+$ leads to more efficient IVR, and thus the IRMPD yield of $[dAdo+H]^+$ is higher than that of $[Ado+H]^+$ in the OPO region above ∼3300 cm^{-1}.

ASSOCIATED CONTENT

Supporting Information

A complete citation for reference number 52. A detailed description complemented by figures displaying the structures of the B3LYP/6-311+G(d,p) low-energy conformers of [dAdo+H]+ and $[Ado+H]^+$ and their 298 K relative Gibbs free energies determined at the B3LYP/6-311+G(2d,2p) and MP2(full)/6-311+G(2d,2p) levels of theory. Comparisons of the measured IRMPD spectra and calculated linear IR spectra in the fingerprint and hydrogen-stretching regions of select low-energy conformers of $[dAdo+H]^+$ and $[Ado+H]^+$. This material is available free of charge via the Internet at http://pubs.acs.org.

DOI: 10.1021/jp509267k
J. Phys. Chem. B 2015, 119, 2795−2805

AUTHOR INFORMATION

Corresponding Author

*E-mail: mrodgers@chem.wayne.edu.

Notes

The authors declare no competing financial interest.

ACKNOWLEDGMENTS

Financial support of this work was provided by the National Science Foundation, Grants OISE-0730072 and CHE-1409420. R.R.W. gratefully acknowledges support from a Wayne State University Thomas C. Rumble Graduate Fellowship. The authors also thank WSU C&IT for computational resources and support. This work is part of the research program of FOM, which is financially supported by the Nederlandse Organisatie voor Wetenschappeklijk Onderzoek (NWO). The skillful assistance of the FELIX staff is gratefully acknowledged.

REFERENCES

(1) Hanus, M.; Ryjacek, F.; Kabelac, M.; Kubar, T.; Bogdan, T. V.; Trygubenko, S. A.; Hobza, P. Correlated *Ab Initio* Study of Nucleic Acid Bases and Their Tautomers in the Gas Phase, in a Microhydrated Environment and in Aqueous Solution. Guanine: Surprising Stabilization of Rare Tautomers in Aqueous Solution. *J. Am. Chem. Soc.* **2003**, *125*, 7678−7688.

(2) Guallar, V.; Douhal, A.; Moreno, M.; Lluch, J. M. DNA Mutations Induced by Proton and Charge Transfer in the Low-lying Excited Singlet Electronic States of the DNA Base Pairs: A Theoretical Insight. *J. Phys. Chem. A* **1999**, *103*, 6251−6256.

(3) Sniden, R. R. *DNA Structure and Function*; Academic Press: San Diego, 1994, pp 15−22.

(4) Hermann, T.; Patel, D. J. Stitching Together RNA Tertiary Architectures. *J. Mol. Biol.* **1999**, *294*, 829−849.

(5) van Dam, L.; Ouwerkerk, N.; Brinkmann, A.; Raap, J.; Levitt, M. H. Solid-State NMR Determination of Sugar Ring Pucker in C-13-Labeled 2′-Deoxynucleosides. *Biophys. J.* **2002**, *83*, 2835−2844.

(6) Rich, A.; Nordheim, A.; Wang, A. H. The Chemistry and Biology of Left-Handed Z-DNA. *J. Annu. Rev. Biochem.* **1984**, *53*, 791−846.

(7) Waalkes, T. P.; Abeloff, M. D.; Ettinger, D. S.; Woo, K. B.; Gehrke, C. W.; Kuo, K. C.; Borek, E. Modified Ribonucleosides As Biological Markers For Patients With Small Cell-Carcinoma of the Lung. *Eur. J. Cancer Clin. Oncol.* **1982**, *18*, 1267−1274.

(8) Mitchell, E. P.; Evans, L.; Schultz, P.; Madsen, R.; Yarbro, J. W.; Gehrke, C. W.; Kuo, K. Modified Nucleosides in Human Serum. *J. Chromatogr.* **1992**, *581*, 31−40.

(9) Perigaud, C.; Gosselin, G.; Imbach, J. L. Stereospecific Synthesis of Chiral Acyclic Analogs of Guanosine. *Bioorg. Med. Chem. Lett.* **1992**, *2*, 677−680.

(10) Perigaud, C.; Gosselin, G.; Imbach, J. L. Nucleoside Analogs As Chemotherapeutic-Agents: A Review. *Nucleosides Nucleotides* **1992**, *11*, 903−945.

(11) McPherson, A.; Jurnak, F.; Wang, A.; Kolpal, F.; Rich, A.; Molineux, I.; Fitzgerald, P. The Structure of A DNA Unwinding Protein and Its Complexes With Oligodeoxynucleotides by X-Ray-Diffraction. *Biophys. J.* **1980**, *32*, 155−173.

(12) Delamaza, L. M.; Carter, B. J. Molecular Structure of Adeno-Associated Virus Variant DNA. *J. Biol. Chem.* **1980**, *255*, 3194−3203.

(13) Guo, Q.; Min, L.; Churchill, M. E. A.; Tullius, T. D.; Kallenbach, N. R. Asymmetric Structure of A Three-Arm DNA Junction. *Biochemistry* **1990**, *29*, 10927−10934.

(14) Pina, B.; Truss, M.; Ohlenbusch, H.; Postma, J.; Beato, M. DNA Rotational Positioning in A Regulatory Nucleosome is Determined By Base Sequence: An Algorithm to Model the Preferred Superhelix. *Nucleic Acids Res.* **1990**, *18*, 6981−6987.

(15) Vanmeervelt, L.; Moore, M. H.; Lin, P. K. T.; Brown, D. M.; Kennard, O. Molecular and Crystal-Structure of d(CGCGmo^{4}CG) − N^4 − Methoxycytosine. Guanine Base-Pairs in Z-DNA. *J. Mol. Biol.* **1990**, *216*, 773−781.

(16) Florian, J.; Leszczynski, J. Theoretical Investigation of the Molecular-Structure of the Pi-Kappa DNA-Base Pair. *J. Biomol. Struct. Dyn.* **1995**, *12*, 1055−1062.

(17) Santamaria, R.; Quirozgutierrez, A.; Juarez, C. Structures and Energetic Properties of B-DNA Nucleotides. *J. Mol. Struct.: THEOCHEM* **1995**, *357*, 161−170.

(18) Triolo, A.; Arcamone, F. M.; Raffaelli, A.; Salvadori, P. Non-Covalent Complexes Between DNA-Binding Drugs and Double-Stranded Deoxyoligonucleotides: A Study by Ionspray Mass Spectrometry. *J. Mass. Spectrom.* **1997**, *32*, 1186−1194.

(19) Wang, Z.; Wan, K. X.; Ramanathan, R.; Taylor, J. S.; Gross, M. L. Structure and Fragmentation Mechanism of Isomeric T-Rich Oligodeoxynucleotides: A Comparison of Four Tandem Mass Spectrometric Methods. *J. Am. Soc. Mass Spectrom.* **1998**, *9*, 683−691.

(20) Cheatham, T. E.; Srinivasan, J.; Case, D. A.; Kollman, P. A. Molecular Dynamics and Continuum Solvent Studies of the Stability of polyG-polyC and polyA-polyT DNA Duplexes in Solution. *J. Biomol. Struct. Dyn.* **1998**, *16*, 265−280.

(21) Kurnikov, I. V.; Tong, G. S. M.; Madrid, M.; Beratan, D. N. Hole Size and Energetics in Double Helical DNA: Competition Between Quantum Delocalization and Solvation Localization. *J. Phys. Chem. B* **2002**, *106*, 7−10.

(22) Rueda, M.; Kalko, S. G.; Luque, F. J.; Orozco, M. The Structure and Dynamics of DNA in the Gas Phase. *J. Am. Chem. Soc.* **2003**, *125*, 8007−8014.

(23) Guo, X. H.; Bruist, M. F.; Davis, D. L.; Bentzley, C. M. Secondary Structural Characterization of Oligonucleotide Strands Using Electrospray Ionization Mass Spectrometry. *Nucleic Acids Res.* **2005**, *33*, 3659−3666.

(24) Balthasart, F.; Plavec, J.; Gabelica, V. Ammonium Ion Binding to DNA G-Quadruplexes: Do Electrospray Mass Spectra Faithfully Reflect the Solution-Phase Species? *J. Am. Soc. Mass Spectrom.* **2013**, *24*, 1−8.

(25) Jaeger, J. A.; Turner, D. H.; Zuker, M. Predicting Optimal and Suboptimal Secondary Structure For RNA. *Methods Enzymol.* **1990**, *183*, 281−306.

(26) Estes, P. A.; Cooke, N. E.; Liebhaber, S. A. A Native RNA Secondary Structure Controls Alternative Splice-Site Selection and Generates 2 Human Growth-Hormone Isoforms. *J. Biol. Chem.* **1992**, *267*, 14902−14908.

(27) Gutell, R. R.; Power, A.; Hertz, G. Z.; Putz, E. J.; Stormo, G. D. Identifying Constraints on the Higher-Order Structure of RNA: Continued Development and Application of Comparative Sequence-Analysis Methods. *Nucleic Acids Res.* **1992**, *20*, 5785−5795.

(28) Davis, D. R. Stabilization of RNA Stacking by Pseudouridine. *Nucleic Acids Res.* **1995**, *23*, 5020−5026.

(29) Jones, S.; Daley, D. T. A.; Luscombe, N. M.; Berman, H. M.; Thornton, J. M. Protein-RNA Interactions: A Structural Analysis. *Nucleic Acids Res.* **2001**, *29*, 943−954.

(30) Gooch, B. D.; Beal, P. A. Recognition of Duplex RNA by Helix-Threading Peptides. *J. Am. Chem. Soc.* **2004**, *126*, 10603−10610.

(31) Koculi, E.; Hyeon, C.; Thirumalai, D.; Woodson, S. A. Charge Density of Divalent Metal Cations Determines RNA Stability. *J. Am. Chem. Soc.* **2007**, *129*, 2676−2682.

(32) Zhang, A. Y. Q.; Bugaut, A.; Balasubramanian, S. A Sequence-Independent Analysis of the Loop Length Dependence of Intramolecular RNA G-Quadruplex Stability and Topology. *Biochemistry* **2011**, *50*, 7251−7258.

(33) Philips, A.; Milanowska, K.; Lach, G.; Boniecki, M.; Rother, K.; Bujnicki, J. M. MetalionRNA: Computational Predictor of Metal-Binding Sites in RNA Structures. *Bioinformatics* **2012**, *28*, 198−205.

(34) Nir, E.; Imhof, P.; Kleinermanns, K.; de Vries, M. S. REMPI Spectroscopy of Laser Desorbed Guanosines. *J. Am. Chem. Soc.* **2000**, *122*, 8091−8092.

(35) Stueber, D.; Grant, D. M. C-13 and N-15 Chemical Shift Tensors in Adenosine, Guanosine Dihydrate, 2′-Deoxythymidine, and Cytidine. *J. Am. Chem. Soc.* **2002**, *124*, 10539−10551.

(36) Wu, R. R.; Yang, B.; Berden, G.; Oomens, J.; Rodgers, M. T. Gas Phase Conformations and Energetics of Protonated 2′-Deoxyguano-

DOI: 10.1021/jp509267k
J. Phys. Chem. B 2015, 119, 2795−2805

sine and Guanosine: IRMPD Action Spectroscopy and Theoretical Studies. *J. Phys. Chem. B* **2014**, *118*, 14774−14784.
(37) Murgia, S.; Lampis, S.; Zucca, P.; Sanjust, E.; Monduzzi, M. Nucleotide Recognition and Phosphate Linkage Hydrolysis at a Lipid Cubic Interface. *J. Am. Chem. Soc.* **2010**, *132*, 16176−16184.
(38) Adelfinskaya, O.; Terrazas, M.; Froeyen, M.; Marliere, P.; Nauwelaerts, K.; Herdewijin, P. Polymerase-Catalyzed Synthesis of DNA From Phosphoramidate Conjugates of Deoxynucleotides and Amino Acids. *Nucleic Acids Res.* **2007**, *35*, 5060−5072.
(39) Knowles, J. R. The Mechanism of Biotin-Dependent Enzymes. *Annu. Rev. Biochem.* **1989**, *58*, 195−221.
(40) Crespo-Hernandez, C. E.; Cohen, B.; Hare, P. M.; Kohler, B. Ultrafast Excited-State Dynamics in Nucleic Acids. *Chem. Rev.* **2004**, *104*, 1977−2019.
(41) Dodge-Kafka, K. L.; Kapiloff, M. S. The mAKAP Signaling Complex: Integration of cAMP, Calcium, and MAP Kinase Signaling Pathways. *Eur. J. Cell Biol.* **2006**, *85*, 593−602.
(42) Belenky, P.; Bogan, K. L.; Brenner, C. NAD^+ Metabolism in Health and Disease. *Trends Biochem. Sci.* **2007**, *32*, 12−19.
(43) Tu, B. P.; Weissman, J. S. Oxidative Protein Folding in Eukaryotes: Mechanisms and Consequences. *J. Cell Biol.* **2004**, *164*, 341−346.
(44) Greco, F.; Liguori, A.; Sindona, G.; Uccella, N. Gas-Phase Proton Affinity of Deoxyribonucleosides and Related Nucleobases by Fast-Atom-Bombardment Tandem Mass-Spectrometry. *J. Am. Chem. Soc.* **1990**, *112*, 9092−9096.
(45) Di Donna, L.; Napoli, A.; Sindona, G.; Athanassopoulos, C. A Comprehensive Evaluation of the Kinetic Method Applied in the Determination of the Proton Affinity of the Nucleic Acid Molecules. *J. Am. Soc. Mass Spectrom.* **2004**, *15*, 1080−1086.
(46) Touboul, D.; Bouchoux, G.; Zenobi, R. Gas-Phase Protonation Thermochemistry of Adenosine. *J. Phys. Chem. B* **2008**, *112*, 11716−11725.
(47) Valle, J. J.; Eyler, J. R.; Oomens, J.; Moore, D. T.; van der Meer, A. F. G.; von Heldon, G.; Meijer, G.; Hendrickson, C. L.; Marshall, A. G.; Blakney, G. T. Free Electron Laser-Fourier Transform Ion Cyclotron Resonance Mass Spectrometry Facility for Obtaining Infrared Multiphoton Dissociation Spectra of Gaseous Ions. *Rev. Sci. Instrum.* **2005**, *76*, 023103-1−023103-7.
(48) Polfer, N. C.; Oomens, J.; Moore, D. T.; von Helden, G.; Meijer, G.; Dunbar, R. C. Infrared Spectroscopy of Phenylalanine Ag(I) and Zn(II) Complexes in the Gas Phase. *J. Am. Chem. Soc.* **2006**, *128*, 517−525.
(49) Polfer, N. C.; Oomens, J. Reaction Products in Mass Spectrometry Elucidated with Infrared Spectroscopy. *Phys. Chem. Chem. Phys.* **2007**, *9*, 3804−3817.
(50) Oepts, D.; van der Meer, A. F. G.; van Amersfoort, P. W. The Free-Electron-Laser User Facility FELIX. *Infrared Phys. Technol.* **1995**, *36*, 297−308.
(51) *HyperChem Computational Chemistry Software Package*, version 5.0; Hypercube, Inc.: Gainsville, FL, 1997.
(52) Frisch, M. J.; Trucks, G. W.; Schlegel, H. B.; Scuseria, G. E.; Robb, M. A.; Cheeseman, J. R.; Scalmani, G.; Barone, V.; Mennucci, B.; Petersson, G. A.; et al. *Gaussian 09*, revision C.01; Gaussian, Inc.: Wallingford, CT, 2009.
(53) Russo, N.; Toscano, M.; Grand, A.; Jolibis, F. Protonation of Thymine, Cytosine, Adenine, and Guanine DNA Nucleic Acid Bases: Theoretical Investigation into the Framework of Density Functional Theory. *J. Comput. Chem.* **1998**, *9*, 989−1000.
(54) Turecek, F.; Chen, X. Protonated Adenine: Tautomers, Solvated Clusters, and Dissociation Mechanisms. *J. Am. Soc. Mass Spectrom.* **2005**, *16*, 1713−1726.
(55) Gidden, J.; Bowers, M. T. Gas-Phase Conformations of Deprotonated and Protonated Mononucleotides Determined by Ion Mobility and Theoretical Modeling. *J. Phys. Chem. B* **2003**, *107*, 12829−12837.
(56) Steill, J. D.; Oomens, J. Gas-Phase Deprotonation of *p*-Hydroxybenzoic Acid Investigated by IR Spectroscopy: Solution-Phase Structure is Retained upon ESI. *J. Am. Chem. Soc.* **2009**, *131*, 13570−13571.
(57) Plutzer, C.; Nir, E.; de Vries, M. S.; Kleinermanns, K. IR-UV Double-Resonance Spectroscopy of the Nucleobase Adenine. *Phys. Chem. Chem. Phys.* **2001**, *3*, 5466−5469.
(58) van Zundert, G. C. P.; Jaeqx, S.; Berden, G.; Bakker, J. M.; Kleinermanns, K.; Oomens, J.; Rijs, A. M. IR Spectroscopy of Isolated Neutral and Protonated Adenine and 9-Methyladenine. *ChemPhysChem* **2011**, *12*, 1921−1927.
(59) Rajabi, K.; Gillis, E. A. L.; Fridgen, T. D. Structures of Alkali Metal Ion-Adenine Complexes by IRMPD Spectroscopy and Electronic Structure Calculations. *J. Phys. Chem. A* **2010**, *114*, 3449−3456.

DOI: 10.1021/jp509267k
J. Phys. Chem. B 2015, 119, 2795−2805